AIP Applied Physics Letters

Silver high-aspect-ratio micro- and nanoimprinting for optical applications

Stefano Buzzi, Matteo Galli, Mario Agio, and Jörg F. Löffler

Citation: Appl. Phys. Lett. **94**, 223115 (2009); doi: 10.1063/1.3142426
View online: http://dx.doi.org/10.1063/1.3142426
View Table of Contents: http://apl.aip.org/resource/1/APPLAB/v94/i22
Published by the American Institute of Physics.

Silver high-aspect-ratio micro- and nanoimprinting for optical applications

Stefano Buzzi,[1] Matteo Galli,[2] Mario Agio,[3] and Jörg F. Löffler[1,a)]
[1]*Laboratory of Metal Physics and Technology, Department of Materials, ETH Zurich, 8093 Zurich, Switzerland*
[2]*Dipartimento di Fisica "A. Volta", Università degli Studi di Pavia, via Bassi 6, 27100 Pavia, Italy*
[3]*Laboratory of Physical Chemistry, ETH Zurich, 8093 Zurich, Switzerland*

(Received 22 March 2009; accepted 5 May 2009; published online 4 June 2009)

Metal direct nanoimprinting is a fabrication technique based on plastic deformation of ductile metals such as silver and gold pressed into a structured rigid mold. While this process can be exploited to manufacture metallic micro- and nanoparts by removing the mold after processing, it can also be used as a metallization method for producing two-dimensional metallo-dielectric composites. Dense silver-pillar arrays with diameters down to 140 nm, aspect ratios up to 13, and excellent uniformity over large areas were fabricated. The sample quality was confirmed by near-infrared optical reflectances of Si–Ag photonic crystals, which showed strong collective surface plasmon-polariton resonances. © *2009 American Institute of Physics*. [DOI: 10.1063/1.3142426]

Metal micro- and nanostructures and their combination with nonmetallic materials are of great interest in nano-optics. This field has emerged in recent years because of the new properties that can be achieved by micro- and nanostructuring of metals. Promising applications in this context are anticipated in, for example, waveguiding, sensing, and devices that exploit a negative effective refractive index.[1–3] However, further potential applications, e.g., in MEMS and microfluidics, are conceivable because of the high mechanical strength of the freestanding silver structures[4] and the possibilities for producing metallic structures of discretionary shape.[5] In this letter we demonstrate the potential of direct metal nanoimprinting for producing optical devices and focus on the fabrication of large arrays of metallic pillars of high aspect ratio, which are particularly challenging to produce.

At the macroscale, imprinting (embossing) is a standard technique for producing metallic components. Difficulties in precise mold fabrication and size effects appearing when structure dimensions become comparable to the metal grains have, however, hindered its application to submicrometer sizes.[6] This difficulty does not apply to amorphous metallic alloys, which can be formed analogously to polymers[7] but such multicomponent alloys possess poor optical properties.[5] Ductile pure metals have rarely been embossed at submicrometer scales[8,9] and never to produce high-aspect-ratio metal projections. This task is considered more difficult than the inverse action, i.e., the imprinting of holes into a metallic surface using mold projections.[10]

We have recently demonstrated, however, that it is possible to reliably produce high-aspect-ratio projections in both silver and gold without size effects in cavity-filling behavior.[5] This is done by applying appropriate forming parameters and, in particular, by processing the metal above its recrystallization temperature. The finding is of great importance for optical applications because gold and silver are the two metals with the lowest absorption in the near-infrared and visible region.[11] Moreover, their outstanding malleability allows the use of relatively mild processing conditions, such that even brittle materials such as silicon, silicon oxide, or silicon nitride can be used as molds. This solves the problems related to precise mold fabrication because of the wide availability of facilities for micro- and nanostructuring of these materials. The latter also have the advantage of being transparent in the near-infrared so that they are easily integrated into optical devices.

Silicon wafers were microstructured by electron-beam lithography and reactive ion etching, except for a macroporous silicon mold produced by lithographic patterning and photoelectrochemical etching at the Max-Planck-Institute in Halle (Germany). The imprinting of 0.2-mm-thick silver plates (Ag 99.9985%, Alfa Aesar) was performed under high vacuum at a temperature of 400 °C and a mechanical pressure of up to 300 MPa. A detailed description of the imprinting process is given in Ref. 5. At this point, two alternative approaches were applied, depending on the goal. On the one hand, if the aim was to release the microstructured silver plate, the silicon mold was chemically removed in a KOH aqueous solution. On the other, to obtain an array of silver rods embedded in the silicon wafer, the excess silver remaining on the mold surface was eliminated. This was done in two steps: an initial rough mechanical removal step using SiC1200 and SiC4000 polishing paper and aluminum scraping (aluminum is harder than silver but softer than silicon), followed by fine chemical-mechanical polishing with a colloidal silica suspension (Logitech Syton SF1). The samples with Ag nanorods in Si were optically characterized by measuring the angle- and polarization-resolved specular reflectance using a Fourier-transform spectrometer (Bruker IFS66).

In the following the nanoimprinting potentials are presented for silver plates after embossing and mold removal. A favorable size effect, resulting in considerably enhanced strength in submicron metallic structures, facilitates this mold removal. The imprinted silver pillars with a diameter of 130 nm, for example, show a compression strength ten times larger than that of pillars with diameters above 1 μm.[4] Figure 1(a) demonstrates the versatility of the nanoimprinting process with an accurate reproduction of all mold cavities with sizes between 130 nm and 4 μm. The magnified view of an array of closely packed, freestanding silver pillars with

a)Electronic mail: joerg.loeffler@mat.ethz.ch.

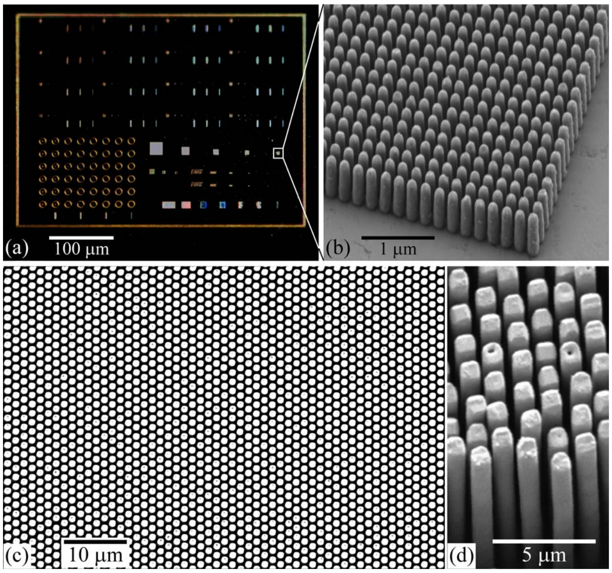

FIG. 1. (Color online) (a) Dark-field optical microscope image showing a silver sample with imprinted arrays of pillars, lines, and other structures after silicon mold removal. (b) Scanning electron microscopy (SEM) closeup of silver pillars with diameter 140 nm, period 200 nm, and height 460 nm. (c) Top-view SEM image of a large-area array of hexagonally packed 1 μm silver pillars with period 1.5 μm and aspect ratio 13, free-standing on a silver plate. (d) Tilted view of a defect region of the sample shown in (c), where the front pillars have been bent, enabling observation of the high aspect ratio and uniform height of the silver structures (which in this region are, however, not perfectly vertical).

a diameter of 140 nm is shown in Fig. 1(b), which illustrates the quality and regularity of the structures. The pillar array of Figs. 1(c) and 1(d) demonstrates the large-area uniformity, including pillar height (13 μm $\pm 5\%$), that can be achieved. In this sample the pillar height is determined by the silver formability and the imprinting parameters since the 100-μm-deep cavities in the macroporous silicon mold were not completely filled; thus, even higher pillar aspect ratios may be achieved with longer compression periods or more elevated pressures. It should also be emphasized that the silicon mold survived the imprinting stress undamaged despite its brittleness and high porosity. Further, the excellent regularity achieved demonstrates that even pillars of very high aspect ratio can be successfully released from the mold and maintain their original vertical shape despite the strong capillary forces that are generated during drying after silicon wet etching.

Arrays similar to those in Fig. 1(b) may find applications in field-emission displays,[12] while arrays of lines may be exploited in polarization filters.[9] The sample in Fig. 1(c) shows that nanoimprinting is suitable for producing pillars with high aspect ratios, even those so high that they can be optically considered as quasi-two-dimensional[13] (this applies to aspect ratios above ~10). This property simplifies simulations and may also generate interesting applications. For example, Wang *et al.*[14] predicted the achievement of a negative refraction for wavelengths around 50 μm using nearly identical gold pillar pairs.

As mentioned earlier, final mold removal is not necessarily desired. In fact, periodic arrays of metallic (e.g., Ag) pillars in a dielectric matrix such as Si, SiO_2, or composite dielectrics with integrated waveguides directing light to the region of the metallic structures, may also be of great interest, e.g., for sensing technology. Two examples of such structures produced by imprinting, consisting of Ag nanorods embedded in a Si matrix, are shown in Fig. 2(a). The filling was complete and very homogeneous over the whole areas of 500×500 μm^2. The samples have sizes and periods similar to those of the gold pillar arrays which Zhang *et al.*[15] pro-

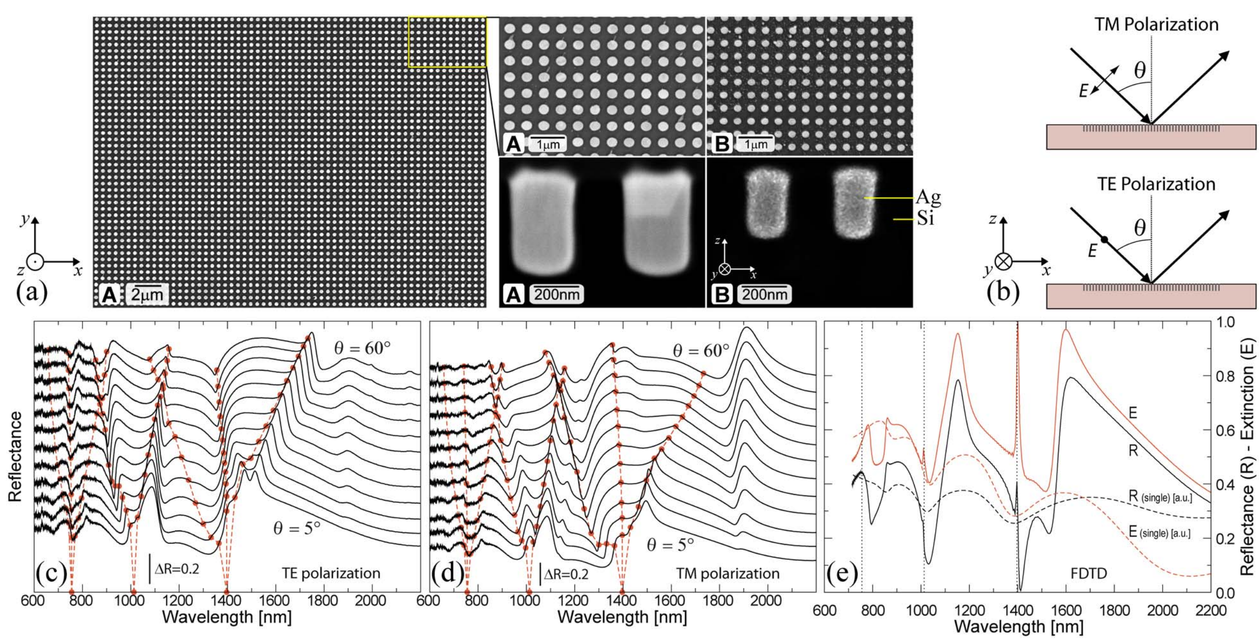

FIG. 2. (Color online) (a) Top-view SEM images and focused ion beam (FIB) cross sections of silver–silicon photonic crystals. Sample A: Ag pillars with diameter $d=285$ nm, period $a=500$ nm, and depth $h=470$ nm (aspect ratio 1.65). Sample B: Ag-pillars with $d=180$ nm, $a=400$ nm, and $h=325$ nm (aspect ratio 1.8). (b) Sketch of the optical reflectance measurements. [(c) and (d)] Variable-angle reflectance spectra of sample B for light with TE and TM polarizations, measured along the Γ-X orientation (incidence plane normal to y-direction), with the incident angle θ varying from 5° to 60° in steps of 5°. The spectra are shifted vertically for clarity. The ΔR bar gives a scale for the reflectance. (e) FDTD simulation of the normal (θ=0°) reflectance (R) and extinction (E) for a single Ag nanorod (dashed line) and a regular array of nanorods (solid line) embedded in Si, taking into account a 2.5-nm-thick native oxide (SiO_2) layer between Ag and Si, with the parameters of sample B.

duced by confining colloidal gold nanoparticles in hole arrays. Besides the associated lower risk of incorporating impurities and porosity in the metallic structures, imprinting offers considerably enhanced design freedom and facilitates the local introduction of inhomogeneities in the periodicity to produce new optical effects.

Figures 2(c) and 2(d) show the angle-resolved reflectance spectra for transverse-electric (TE) and transverse-magnetic (TM) polarization [see Fig. 2(b)]. The spectra are characterized by the presence of sharp and asymmetric resonances, which show a clear dispersion in energy as a function of the incidence angle. The resonances in sample A (not shown) are analogous to those of sample B but shifted toward lower frequencies due to the larger pillars and period. This peculiar optical response is indeed very similar to that observed in all-dielectric slab photonic crystals,[16] where the sharp resonances in reflectance spectra are directly related to the excitation of quasi-guided photonic modes in the periodic structure. The strong resonant features observed in our array of metal nanoparticles are related to both the excitation of localized surface plasmon-polariton resonances (LSPRs) of the individual Ag nanorods, and collective surface plasmon-polariton resonances (CSPRs) supported by the nanoparticle array.[17,18] The wavelength of the CSPRs observed is set by the Rayleigh cutoff for diffraction into the substrate

$$\lambda = a\frac{n^2 - \sin^2\theta}{i\sin\theta + \sqrt{i^2\sin^2\theta + (i^2+j^2)(n^2-\sin^2\theta)}}, \tag{1}$$

where n is the index of refraction of the Si substrate, θ is the angle of incidence, and a is the array period. The integers i and j refer to the diffraction order along the x and y axes.

The full circles in Figs. 2(c) and 2(d) label the position of the CSPRs as given by Eq. (1) for the first diffraction orders $(i,j)=(0,\pm 1)$, $(\pm 1,0)$, $(\pm 1,\pm 1)$, $(0,\pm 2)$, and $(\pm 2,0)$. Their vertical position corresponds to the value of the measured reflectance at the wavelength of the CSPR. The full circles on the horizontal axis refer to the case $\theta=0°$. Note that the position and dispersion of the experimental curves agrees well with the values of Eq. (1) only if the dispersion of Si is taken into account.[11] The linewidth, lineshape, and strength of the CSPRs depend on several parameters and will be the subject of further investigations. Contrary to previous works,[17,18] which used Au nanoparticle arrays on low-index substrates, the current samples made of Ag nanorods in a high-index material enable the mapping of several CSPRs due to different diffraction orders in the near-infrared spectral range. The reflectance curves also contain information on the LSPRs. Because their spectral position overlaps with the diffraction-related CSPRs, it is difficult to isolate them, also because the high-index substrate makes them quite broad except for the isolated LSPR around 1900 nm. The latter corresponds to an excitation along the z-axis of the nanorods when the incident angle increases and the light is TM polarized [Fig. 2(d)]. The absence of resonances originating from the dielectric structure was confirmed by equivalent measurements performed on the same samples before silver filling (empty air holes), which showed a nearly flat optical response (not shown).

To better understand the role of the other LSPRs, finite-difference time-domain (FDTD) simulations[19] of arrays and isolated nanorods were performed using normal incident light. Figure 2(e) compares the extinction and reflection spectra computed using the nominal parameters of sample B (solid curves) with those of a single silver nanorod under the same conditions (dashed curves). The CSPRs (vertical dotted lines) are clearly not present in the single-nanoparticle spectra. The LSPRs are broad, as expected, and their peak position and linewidth alter[17] when they are coupled with the CSPRs in the array. The experimental TE and TM curves obtained for $\theta=5°$ should be similar to the FDTD results for normal incidence. The position of the resonances, the lineshape and linewidth, indeed show good agreement. The difficulty of knowing the exact geometric parameters, size dispersion, and other structural disorders in the sample explain the small discrepancy.

In conclusion, we have demonstrated the great potential of direct imprinting for producing large-scale, high-quality arrays of Ag micro- and nanopillars. The process is especially attractive for achieving very high aspect ratios with dense metallic structures. Reflectance measurements of square arrays of Ag nanorods produced by imprinting exhibited strong CSPRs, confirming the uniformity and high quality of the periodic metallic structures. This is encouraging for the technique's application in the production of optical devices.

The authors are grateful to A. Sologubenko, L. Zhao, R. Giannini, M. Liscidini, and L. C. Andreani for technical support and helpful discussions. M. A. thanks V. Sandoghdar for continuous support. This work was financed by the ETH Zurich Initiative on Composite Doped Metamaterials (CDM) and by ETH research Grant No. TH-29/07-3.

[1]W. L. Barnes, A. Dereux, and T. W. Ebbesen, Nature (London) **424**, 824 (2003).
[2]J. N. Anker, W. P. Hall, O. Lyandres, N. C. Shah, J. Zhao, and R. P. Van Duyne, Nature Mater. **7**, 442 (2008).
[3]D. R. Smith, J. B. Pendry, and M. C. K. Wiltshire, Science **305**, 788 (2004).
[4]S. Buzzi, M. Dietiker, K. Kunze, R. Spolenak, and J. F. Löffler, Philos. Mag. **89**, 869 (2009).
[5]S. Buzzi, F. Robin, V. Callegari, and J. F. Löffler, Microelectron. Eng. **85**, 419 (2008).
[6]U. Engel and R. Eckstein, J. Mater. Process. Technol. **125**, 35 (2002).
[7]G. Kumar, H. X. Tang, and J. Schroers, Nature (London) **457**, 868 (2009).
[8]S. W. Pang, T. Tamamura, M. Nakao, A. Ozawa, and H. Masuda, J. Vac. Sci. Technol. B **16**, 1145 (1998).
[9]Y. Hirai, T. Ushiro, T. Kanakugi, and T. Matsuura, Proc. SPIE **5220**, 74 (2003).
[10]H. Ike and M. Plancak, J. Mater. Process. Technol. **80**, 101 (1998).
[11]*Handbook of Optical Constants of Solids*, edited by E. D. Palik (Academic, New York, 1997).
[12]T. Kim, J. Kim, S. J. Son, and S. Seo, Nanotechnology **19**, 295302 (2008).
[13]H. van der Lem and A. Moroz, J. Opt. A, Pure Appl. Opt. **2**, 395 (2000).
[14]F. M. Wang, H. Liu, T. Li, Z. G. Dong, S. N. Zhu, and X. Zhang, Phys. Rev. E **75**, 016604 (2007).
[15]X. Zhang, B. Sun, H. Guo, N. Tetreault, H. Giessen, and R. H. Friend, Appl. Phys. Lett. **90**, 133114 (2007).
[16]M. Patrini, M. Galli, F. Marabelli, M. Agio, L. C. Andreani, D. Peyrade, and Y. Chen, IEEE J. Quantum Electron. **38**, 885 (2002).
[17]V. G. Kravets, F. Schedin, and A. N. Grigorenko, Phys. Rev. Lett. **101**, 087403 (2008).
[18]B. Auguie and W. L. Barnes, Phys. Rev. Lett. **101**, 143902 (2008).
[19]The FDTD simulations take into account the material dispersion of silver and silicon through appropriate dispersion models.